

Hyperpolarization

Hyperpolarizing Concentrated Metronidazole $^{15}\text{NO}_2$ Group over Six Chemical Bonds with More than 15 % Polarization and a 20 Minute Lifetime

Roman V. Shchepin,^[a] Jonathan R. Birchall,^[b] Nikita V. Chukanov,^[c, d] Kirill V. Kovtunov,^[c, d] Igor V. Koptyug,^[c, d] Thomas Theis,^[e] Warren S. Warren,^[f] Juri G. Gelovani,^[b] Boyd M. Goodson,^[g] Sepideh Shokouhi,^[a] Matthew S. Rosen,^[h] Yi-Fen Yen,^[h] Wellington Pham,^[a] and Eduard Y. Chekmenev^{*,[b, i]}

Abstract: The NMR hyperpolarization of uniformly ^{15}N -labeled [$^{15}\text{N}_3$]metronidazole is demonstrated by using SABRE-SHEATH. In this antibiotic, the $^{15}\text{NO}_2$ group is hyperpolarized through spin relays created by ^{15}N spins in [$^{15}\text{N}_3$]metronidazole, and the polarization is transferred from parahydrogen-derived hydrides over six chemical bonds. In less than a minute of parahydrogen bubbling at approximately 0.4 μT , a high level of nuclear spin polarization ($P_{^{15}\text{N}}$) of around 16% is achieved on all three ^{15}N sites. This prod-

uct of ^{15}N polarization and concentration of ^{15}N spins is around six-fold better than any previous value determined for ^{15}N SABRE-derived hyperpolarization. At 1.4 T, the hyperpolarized state persists for tens of minutes (relaxation time, $T_1 \approx 10$ min). A novel synthesis of uniformly ^{15}N -enriched metronidazole is reported with a yield of 15%. This approach can potentially be used for synthesis of a wide variety of in vivo metabolic probes with potential uses ranging from hypoxia sensing to theranostic imaging.

[a] Prof. Dr. R. V. Shchepin, Prof. Dr. S. Shokouhi, Prof. Dr. W. Pham
Department of Radiology, Vanderbilt University Institute of Imaging Science (VUIIS), Vanderbilt University Medical Center (VUMC)
Nashville, Tennessee 37232-2310 (USA)

[b] Dr. J. R. Birchall, Prof. Dr. J. G. Gelovani, Prof. Dr. E. Y. Chekmenev
Department of Chemistry, Integrative Biosciences (Ibio)
Karmanos Cancer Institute (KCI), Wayne State University
Detroit, Michigan 48202 (USA)
E-mail: chekmenev@wayne.edu

[c] Dr. N. V. Chukanov, Dr. K. V. Kovtunov, Prof. Dr. I. V. Koptyug
International Tomography Center, SB RAS
3A Institutskaya St., Novosibirsk 630090 (Russia)

[d] Dr. N. V. Chukanov, Dr. K. V. Kovtunov, Prof. Dr. I. V. Koptyug
Novosibirsk State University
2 Pirogova St., Novosibirsk 630090 (Russia)

[e] Prof. Dr. T. Theis
Department of Chemistry, North Carolina State University
Raleigh, North Carolina, 27695-8204 (USA)

[f] Prof. Dr. W. S. Warren
Department of Chemistry, Duke University
Durham, North Carolina 27708 (USA)

[g] Prof. Dr. B. M. Goodson
Department of Chemistry and Biochemistry and
Materials Technology Center, Southern Illinois University
Carbondale, Illinois 62901 (USA)

[h] Prof. Dr. M. S. Rosen, Prof. Dr. Y.-F. Yen
Massachusetts General Hospital
Athinoula A. Martinos Center for Biomedical Imaging
Boston, Massachusetts 02129 (USA)

[i] Prof. Dr. E. Y. Chekmenev
Russian Academy of Sciences
Leninskiy Prospekt 14, Moscow, 119991 (Russia)

 Supporting information and the ORCID identification number(s) for the author(s) of this article can be found under:
<https://doi.org/10.1002/chem.201901192>

Introduction

NMR hyperpolarization techniques transiently increase nuclear spin polarization (P) by several orders of magnitude.^[1–3] This significant increase in P enables metabolic magnetic resonance spectroscopy (MRS) and MRS imaging (MRSI) after a bolus injection of a hyperpolarized (HP) compound to detect abnormal metabolism in cancer and other diseases.^[4–10] The ^{13}C isotope has been widely employed in a number of biomolecules, most notably in [$1\text{-}^{13}\text{C}$]pyruvate,^[6,8] which is typically hyperpolarized by dissolution dynamic nuclear polarization (d-DNP).^[11,12] However, this approach has a number of shortcomings. First, the lifetime of the HP state (governed by the spin–lattice constant of exponential decay) is relatively short [e.g., compared with those of ^{18}F and ^{11}C positron emission tomography (PET) tracers], with the relaxation time (T_1) on the order of 1 min.^[13] As a result, only a limited number of metabolic pathways are amenable to MRSI, because sufficient levels of nuclear spin polarization must persist until detection.^[11,14] Secondly, d-DNP generally requires several tens of minutes (or longer) of hyperpolarization buildup time as well as sophisticated, costly equipment.^[15,16]

The hyperpolarization of ^{15}N sites in biomolecules is a viable alternative approach,^[17–19] because ^{15}N sites can generally retain nuclear spin polarization for significantly longer periods of time, with T_1 values of more than 10 minutes having been observed in quaternary nitrogen sites in several model compounds.^[20,21] However, HP ^{15}N -labeled choline (along with its derivatives) is the only quaternary amine with biomedical rele-

vance in the context of HP MRS.^[22] Unfortunately, the small difference in chemical shift observed for [¹⁵N]choline and its metabolites (ca. 0.2 ppm) would make them difficult to distinguish *in vivo*.^[5,22] On the other hand, nitro groups occur in a wide range of drugs approved by the US Food and Drug Administration (FDA), including antibiotics, cancer radio-sensitizing agents,^[23] hypoxia sensors,^[24] and chemotherapeutics,^[25] and can therefore potentially serve as convenient biocompatible moieties to retain the HP state for tens of minutes.

Signal amplification by reversible exchange (SABRE) is a hyperpolarization technique that employs parahydrogen as the source of hyperpolarization.^[26–33] In this work we employed the SABRE in the shield enables alignment transfer to heteronuclei (SABRE-SHEATH)^[34,35] variant of SABRE, which relies on simultaneous chemical exchange between parahydrogen (pH₂) and the to-be-hyperpolarized biomolecules (without altering their structures) within the ligand sphere of a catalyst in microtesla (μT) magnetic fields (Figure 1a). SABRE-SHEATH has been shown to produce ¹⁵N HP states with *P* values of up to 30% in under 1 minute (although these high polarization levels have

previously been obtained at a relatively low concentration of ¹⁵N spins).^[36–38] Unlike d-DNP,^[12] SABRE-SHEATH requires relatively simple and inexpensive hardware.^[34,35]

Results and Discussion

Although to date ¹⁵N hyperpolarization of several biomolecules has been demonstrated by SABRE-SHEATH, which opens up a range of potential contrast agents,^[38] nearly all previous reports have focused on the hyperpolarization of ¹⁵N sites that directly interact with the iridium catalytic center of the Ir-IMes (IMes = 1,3-dimesitylimidazol-2-ylidene) polarization transfer catalyst, which is the catalyst typically used in most SABRE experiments.^[39] The direct polarization transfer from pH₂-derived hydrides to these ¹⁵N sites is efficient (i.e., fast and yielding high values of *P*_{15N}), because the two-bond ¹H–¹⁵N spin–spin couplings are relatively strong (e.g., 10–20 Hz) and sufficiently different from each other as to render the exchangeable catalyst binding sites magnetically inequivalent from one another.^[34,35]

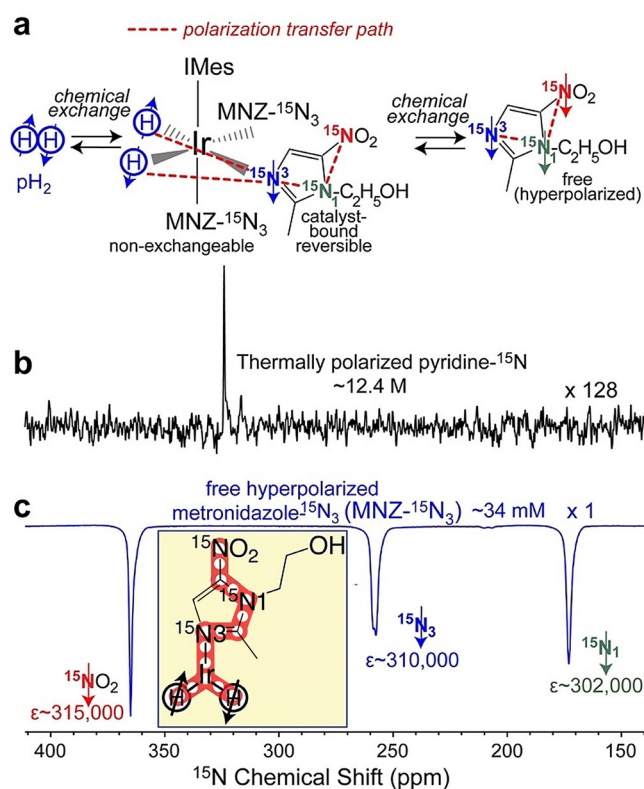


Figure 1. a) Schematic of the simultaneous chemical exchange of pH₂ and [¹⁵N₃]metronidazole (MNZ-¹⁵N₃) on the Ir-IMes polarization transfer catalyst.^[39] Note the dashed red lines indicate the likely path of spin-relayed polarization transfer from pH₂-derived hydrides to the ¹⁵NO₂ group via the ¹⁵N₃ and ¹⁵N₁ sites. b) Single-scan ¹⁵N NMR signal reference spectrum of thermally polarized neat (no solvent) [¹⁵N]pyridine (12.4 M). c) Single-scan ¹⁵N NMR spectrum of HP [¹⁵N₃]metronidazole in [D₄]MeOH. All NMR spectra were recorded at 1.4 T. The inset displays (in red) the path of chemical bonds over which the network of *I* = 1/2 spin relays is established. The following experimental conditions were employed for SABRE-SHEATH hyperpolarization: Room temperature, 6.7 atm overpressure of the medium-walled NMR tube, and a flow rate of 70 sccm (standard cubic centimeters per minute) of pH₂ controlled by a mass-flow controller (MFC).

Spin-relayed polarization transfer

Although in general direct SABRE-SHEATH of remote spin *I* = 1/2 sites over three or more chemical bonds is inefficient,^[40] we have recently demonstrated the concept of spin-relayed polarization transfer from SABRE-SHEATH-hyperpolarized ¹⁵N sites to other ¹³C and ¹⁵N sites within the same molecule.^[41–43] In this approach, a network of *J*-coupled spin *I* = 1/2 nuclei can transmit polarization several chemical bonds away from the pH₂-derived hydrides.^[41,42]

In this paper we show that uniformly ¹⁵N-labeled [¹⁵N₃]metronidazole (MNZ-¹⁵N₃) can be efficiently hyperpolarized by the SABRE-SHEATH approach to *P*_{15N} > 16% for each of the three ¹⁵N sites by using 87% pH₂. Figure 1c shows the spectrum of HP MNZ-¹⁵N₃, in which all three ¹⁵N peaks are dramatically enhanced, with ¹⁵N polarization increased by over 300 000-fold compared with thermal ¹⁵N polarization (for an NMR spectrum of a thermally polarized signal reference compound at 1.4 T, see Figure 1b). The signal enhancements are field-dependent, because thermal polarization varies linearly with the applied magnetic field. We note that four-, five- and six-bond spin–spin couplings between pH₂-derived ¹⁵N hydrides and ¹⁵N₁ and ¹⁵N₂ sites, respectively, are negligible, and therefore direct polarization transfer is highly inefficient, as described previously.^[37] Analysis of the ¹⁵N–¹⁵N spin–spin couplings in MNZ-¹⁵N₃ (see Figure S2 in the Supporting Information) revealed *J*_{15N–15N} values of around 1.65 Hz between the ¹⁵N₃ and ¹⁵N₁ sites and around 1.45 Hz between the ¹⁵N₁ and ¹⁵N₂ sites. No spin–spin coupling between the ¹⁵N₂ and ¹⁵N₃ sites was detected. Therefore, we conclude that the ¹⁵N₃ site is likely hyperpolarized first by SABRE-SHEATH from pH₂-derived hydrides, the ¹⁵N₁ site is hyperpolarized next by spin-relayed polarization transfer from the HP ¹⁵N₃ site, and the ¹⁵N₂ site is hyperpolarized last by spin-relayed transfer from the ¹⁵N₁ site. We note that the ¹⁵N₂ site is not significantly spin–spin cou-

pled to any other nucleus besides $^{15}\text{N}1$, further supporting our conclusion.

^{15}N polarization dynamics

Studies of the polarization field dependence, dynamics, and decay for $^{15}\text{N}_3$ metronidazole are summarized in Figure 2. In part because the $^{15}\text{NO}_2$ site is effectively isolated from protons in the $^{15}\text{N}_3$ metronidazole molecule, we found that it has a significantly longer T_1 (9.7 ± 1.0 min) than the $^{15}\text{N}3$ (3.1 ± 0.4 min) and $^{15}\text{N}1$ (3.8 ± 0.3 min) sites, respectively (Figure 2f). The relayed (versus direct) nature of the polarization transfer mechanism is also supported by the magnetic field dependence (Figure 2a) of $P_{15\text{N}}$ for the three ^{15}N sites, which reveals that the maxima of $P_{15\text{N}}$ for the $^{15}\text{NO}_2$ and $^{15}\text{N}1$ sites coincide with that for the $^{15}\text{N}3$ site, which is consistent with the notion that the

$^{15}\text{N}3$ site acts as the local source of polarization. Moreover, the kinetics of ^{15}N polarization buildup at the optimal magnetic field (ca. $0.4 \mu\text{T}$) clearly indicates that, during the buildup process, $P_{15\text{N}3} > P_{15\text{N}1} > P_{15\text{NO}_2}$ (Figure 2b). It is worth noting that the three $P_{15\text{N}}$ values tend towards similar values when the buildup is nearly complete (Figure 2a). On the other hand, during the ^{15}N polarization decay process in a field of around $0.4 \mu\text{T}$, this order of $P_{15\text{N}}$ values is reversed, that is, $P_{15\text{N}3} < P_{15\text{N}1} < P_{15\text{NO}_2}$ (Figure 2e). It is also worth noting that when the magnetic field is below the optimal value (left-hand slope in Figure 2a), the $^{15}\text{N}3$ site is hyperpolarized better than the $^{15}\text{N}1$ and $^{15}\text{NO}_2$ sites. The lower levels of polarization observed below $0.4 \mu\text{T}$ and the fact that the polarization of $^{15}\text{N}1$ is lower than that of $^{15}\text{N}3$ are likely explained by the “strong coupling” of protons and heteronuclei in magnetic fields in the range $100 \text{ nT} - 1 \mu\text{T}$ observed by Kiryutin et al.,^[44] which may lead to more efficient depolarization of the $^{15}\text{N}1$ site, which is coupled more efficiently to the proton spin network (see the Supporting Information for details) compared with the $^{15}\text{N}3$ site. Because ^{15}N polarization of the $^{15}\text{NO}_2$ site is dependent on that of $^{15}\text{N}1$ (because the strongest spin–spin coupling of the $^{15}\text{NO}_2$ site is with the $^{15}\text{N}1$ site), the lower ^{15}N polarization of the $^{15}\text{NO}_2$ site (compared with that of the $^{15}\text{N}3$ site) is also expected. We have employed the nonequal HP spin-state condition, that is, $P_{15\text{N}3} > P_{15\text{N}1} > P_{15\text{NO}_2}$, to study the dynamics of polarization evolution in the Earth’s magnetic field (ca. $30 \mu\text{T}$), in which pH_2 can no longer efficiently hyperpolarize any heteronuclei and therefore the polarization can only decay.^[34,35,45] Figure 2c shows that $P_{15\text{N}3}$ is redistributed relatively quickly, on the timescale of seconds, to the $^{15}\text{N}1$ and $^{15}\text{NO}_2$ sites (it is worth noting that $P_{15\text{N}1}$ and $P_{15\text{NO}_2}$ grow for the first approx. 15 s, whereas $P_{15\text{N}3}$ decreases). Although this redistribution of polarization occurs in the Earth’s magnetic field, which is approximately $30 \mu\text{T}$ (as measured in our laboratory) and significantly exceeds $0.4 \mu\text{T}$, this observation provides additional support for the spin-relayed mechanism of SABRE-SHEATH polarization transfer in $^{15}\text{N}_3$ metronidazole in microtesla magnetic fields.

^{15}N polarization levels

It should be noted that over the MNZ concentration range studied ($23 - 41 \text{ mM}$), $P_{15\text{N}}$ was $15.6 \pm 0.7\%$ on all three ^{15}N sites, as detected by 1.4 T NMR spectroscopy (Figure 2d; notably, the ratio of MNZ and the catalyst was maintained constant at $20:1$). This polarization level is lower (by around two-fold) than the best $P_{15\text{N}}$ values (ca. 34%) obtained for metronidazole with a natural abundance of ^{15}N ($< 0.3\%$) under similar conditions (Figure 3a).^[36] This observation can likely be explained by two effects: First, the labeled compound produces an active complex with two ^{15}N sites in the equatorial plane and the polarization is transferred in the AA’BB’ four-spin system, whereas in the case of metronidazole with a natural abundance of ^{15}N , polarization transfer from the pH_2 -derived hydrides to ^{15}N occurs in an AA’B three-spin system. It has been shown previously that polarization transfer in such three-spin systems may be more efficient than that in four-spin systems.^[34,35,45,46] The second contributing factor is access to fresh pH_2 , which can be

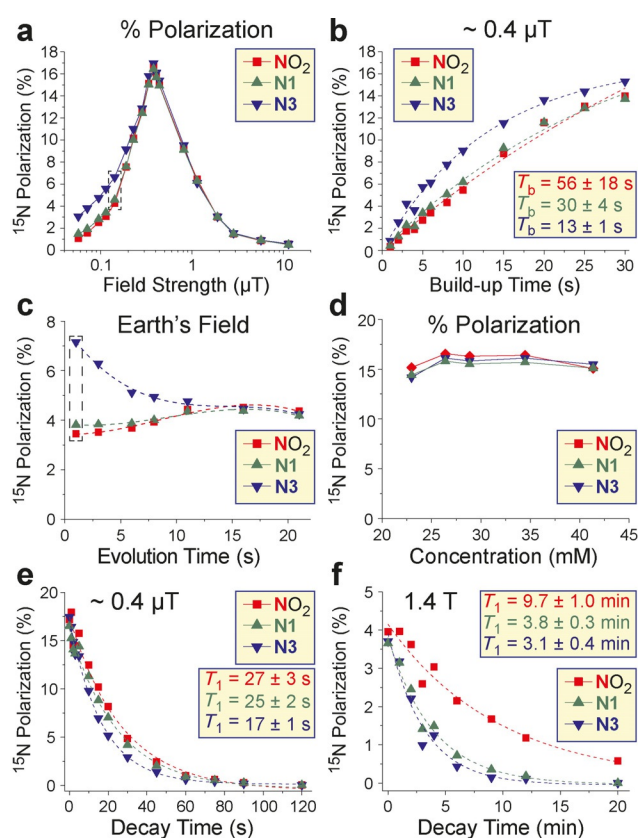


Figure 2. Studies of SABRE-SHEATH hyperpolarization of $^{15}\text{N}_3$ metronidazole (MNZ- $^{15}\text{N}_3$) by using NMR spectroscopy at 1.4 T . a) Dependence of $P_{15\text{N}}$ on the magnetic field for the three ^{15}N sites. b) Dynamics of $P_{15\text{N}}$ at the three ^{15}N sites at approx. $0.4 \mu\text{T}$ with single-exponential fitting. Note that the buildup of $P_{15\text{N}}$ at the $^{15}\text{NO}_2$ and $^{15}\text{N}1$ sites is not well described by mono-exponential growth due to the complex dynamics of the buildup process at multiple sites (the mono-exponential buildup curves and time constants are provided for comparative purposes (with respect to the $^{15}\text{N}3$ site) only). c) Evolution of $P_{15\text{N}}$ at the three ^{15}N sites in the Earth’s magnetic field (ca. $30 \mu\text{T}$) using the initial conditions of $P_{15\text{N}3} > P_{15\text{N}1} > P_{15\text{NO}_2}$ (the initial points within the dashed box correspond to those in (a), denoting the magnetic field of HP state preparation). d) Concentration dependence of $P_{15\text{N}}$ at the three ^{15}N sites. e) Decay of $P_{15\text{N}}$ at the three ^{15}N sites at approx. $0.4 \mu\text{T}$. The sample was transferred to a 1.4 T NMR spectrometer for detection. f) Decay of $P_{15\text{N}}$ at the three ^{15}N sites at 1.4 T . The color coding indicates the three ^{15}N sites: $^{15}\text{N}1$: green; $^{15}\text{N}3$: blue; $^{15}\text{NO}_2$: red.

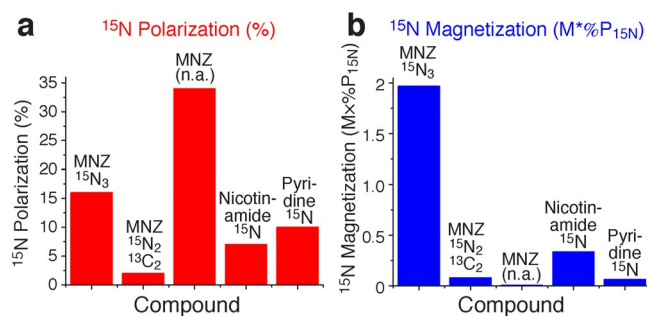


Figure 3. a) ¹⁵N polarization and b) ¹⁵N magnetization, defined as the product of the molar concentration of ¹⁵N spins in the HP substrate and ¹⁵N polarization, in [¹⁵N₃]metronidazole (MNZ-¹⁵N₃) studied here, [¹⁵N₂, ¹³C₂]metronidazole (MNZ-¹⁵N₂, ¹³C₂),^[41] natural abundant metronidazole [MNZ (n.a.)],^[36] mono-¹⁵N-labeled [¹⁵N₁]nicotinamide,^[36] and [¹⁵N]pyridine.^[34] Note the multiple spin labels in some compounds.

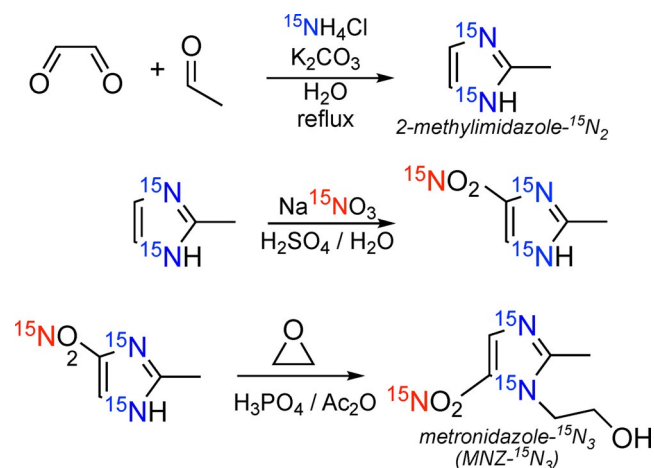
more limited under conditions of high ¹⁵N density (i.e., local p_{H₂} can be depleted more quickly if there are more ¹⁵N sites present),^[45] the labeled sample studied here contains more than 600-fold more ¹⁵N sites than the natural abundance compound studied previously.^[36]

¹⁵N polarization payload and ¹⁵N magnetization

Comparison of the polarization payload (defined as the product of the concentration of ¹⁵N spins, ¹⁵N polarization, and the volume of the HP contrast agent) is more relevant in the context of biomedical applications, because in vivo experiments greatly benefit from a higher HP payload to enhance the signal-to-noise ratio and improve spatial and temporal resolution.^[47] Because SABRE is a highly scalable hyperpolarization technique (i.e., varying the volume of HP liquids is relatively straightforward), it is important to highlight the ¹⁵N magnetization achieved, that is, the product of ¹⁵N spin concentration and ¹⁵N polarization. The ¹⁵N polarization levels of several biomolecules hyperpolarized by SABRE are compared in Figure 3a, and the ¹⁵N magnetization determined for the same five compounds hyperpolarized by SABRE are presented in Figure 3b. The ¹⁵N magnetization for [¹⁵N₃]metronidazole is improved by around 25-fold or more compared with the previously studied molecules [i.e., compared with MNZ(n.a.) and MNZ-¹⁵N₂, ¹³C₂].^[36] Moreover, the ¹⁵N magnetization calculated here for [¹⁵N₃]metronidazole is approximately six-fold greater than that of mono-¹⁵N-labeled [¹⁵N]nicotinamide.^[34]

Synthesis of ¹⁵N-enriched metronidazole

Importantly, the above NMR results were enabled by ¹⁵N enrichment of all three nitrogen sites of the substrate, achieved by a novel but straightforward spin-labeling synthetic procedure (Scheme 1). First, 2-methyl[¹⁵N₂]imidazole was prepared by using a modification of the procedure previously developed for the synthesis of [¹⁵N₂]imidazole,^[48] in which inexpensive ¹⁵NH₄Cl was employed as the ¹⁵N source. In the second step, the ¹⁵NO₂ group was added by a nitration reaction using Na¹⁵NO₃ as the second inexpensive ¹⁵N source. Ethylene oxide



Scheme 1. Three-step ¹⁵N-enrichment of [¹⁵N₃]metronidazole (MNZ-¹⁵N₃). Note the color coding of the ¹⁵N sources, ¹⁵NH₄Cl and Na¹⁵NO₃, the color coding (blue and red, respectively) in the products indicating the source of the ¹⁵N label.

was employed in the last step to introduce the hydroxyethyl moiety. The overall yield over three steps (Scheme 1) was around 15% (see Section 9 of the Supporting Information). This synthetic approach for introducing ¹⁵N spin into the nitroimidazole moiety can be potentially applied to a wide range of nitroimidazole-based drugs, for example, azomycin, benznidazole, secnidazole, ornidazole, nimorazole, TH-4000, and evofosfamide, used as hypoxia sensors, radio-sensitizing therapeutics, and theranostic imaging agents.^[25]

Biomedical outlook

Metronidazole is an FDA-approved antibiotic that can be safely administered orally and intravenously in large (multigram) doses.^[49] Moreover, we have recently reported the preparation of pure (i.e., catalyst-free) HP metronidazole solutions^[36] as well as heterogeneous ¹⁵N SABRE-SHEATH^[50] and ¹⁵N SABRE-SHEATH HP metronidazole in aqueous media,^[51] thereby potentially enabling the preparation of biologically compatible HP MNZ-¹⁵N₃ injectable formulation(s). We envision this contrast agent to have potential in hypoxia sensing (the focus of our future studies) in a manner similar to that of [¹⁸F]fluoromisonidazole (FMISO) and other nitro-containing radiotracers employed in positron emission tomography (PET).^[52,53] The nitroimidazole moiety is chemically reduced in the hypoxic environment by upregulated nitroreductases (i.e., in tumors or ischemic tissues),^[24,54] which will likely result in large (tens of ppm) changes in the ¹⁵N chemical shifts of the three ¹⁵N sites. Although future studies are required to investigate the utility of HP MNZ-¹⁵N₃ for hypoxia sensing and other applications, the results presented here ($P_{15N} \approx 16\%$ at $\geq 98\%$ ¹⁵N enrichment, $T_1 \approx 10$ min, fast polarization, and straightforward isotopic enrichment) bode well for such envisioned cellular and in vivo experiments. Moreover, an in vivo study of ¹⁵N relaxation with HP choline revealed an approximate 1.35-fold decrease in T_1 (from 172 ± 16 to 126 ± 15 s) compared with that in vitro at 9.4 T.^[22] The effective reduction of the ¹⁵N T_1

value for HP choline in vivo was attributed to choline uptake and metabolism versus depolarization,^[22] which indicates that the ^{15}N T_1 value is reduced marginally in vivo compared with in vitro, largely because of the very low gyromagnetic ratio of ^{15}N spin (a tenth of that of proton spins). Therefore, we anticipate a relatively small (30% or less) reduction in the T_1 values presented here for [$^{15}\text{N}_3$]metronidazole in future in vivo studies.

Although the level of ^{15}N polarization obtained here is lower than the ^{13}C polarization obtained by using d-DNP hyperpolarizers (^{13}C polarization, ca. 40%^[47]), the amount of actual polarization at the time of MR image acquisition will likely exceed that of ^{13}C , because the $^{15}\text{NO}_2$ group of [$^{15}\text{N}_3$]metronidazole has a significantly longer T_1 (by approximately an order of magnitude) and therefore will enjoy disproportionately lower depolarization during injection, circulation, and imaging. For example, the current time for injection of HP contrast agents in humans is around 55 s,^[47] which causes an approximate three-fold decay of the ^{13}C polarization level, whereas the $^{15}\text{NO}_2$ polarization of HP [$^{15}\text{N}_3$]metronidazole will decay only by roughly 1.1-fold in that time, that is, it will experience a negligible loss.

However, the low gyromagnetic ratio of ^{15}N spins, which in part endows the long T_1 values demonstrated here, is a double-edged sword, because the NMR detection of low- γ nuclei is generally significantly less sensitive even at the same nominal polarization level.^[55,56] The detected signal is directly proportional to the nuclear magnetic moment (which varies linearly with gyromagnetic ratio), and the NMR signal is also directly proportional to the resonance frequency (which also varies linearly with gyromagnetic ratio). Therefore, it follows that proton detection is around 100 times more sensitive than ^{15}N detection, $(\gamma_{\text{H}}/\gamma_{\text{15N}})^2 \approx 100$, and ^{13}C detection is approximately six times more sensitive than ^{15}N detection, $(\gamma_{\text{13C}}/\gamma_{\text{15N}})^2 \approx 6$. Moreover, in the case of MRI and MRSI applications, spatial imaging encoding of low- γ nuclei carries two additional disadvantages. First, the gradient strength required to achieve the same spatial resolution is directly proportional to the gyromagnetic ratio (and therefore ^{15}N imaging requires ca. 2.5-fold greater gradient strength than ^{13}C imaging and ca. 10-fold greater gradient strength than ^1H imaging). Secondly, the gradient ramp rate is also directly proportional to the gyromagnetic ratio, thereby making gradient rise/fall durations of ^{15}N imaging around 2.5-fold slower than those of ^{13}C imaging and around 10-fold slower than those of ^1H imaging at a fixed gradient strength (i.e., the condition of maximum gradient power).

To summarize, ^{15}N MRI and MRSI face significant fundamental challenges. However, we envision proton detection of ^{15}N HP contrast agents in general and HP [$^{15}\text{N}_3$]nitroimidazole in particular, similarly to the concept of indirect proton detection recently introduced for ^{13}C HP contrast agents,^[17,57–59] which means that the detection sensitivity of ^{15}N HP agents will be similar to that of ^{13}C HP agents when indirect (^1H) proton detection is employed. [$^{15}\text{N}_3$]Metronidazole has protons in its molecular structure that are weakly (2–9 Hz) coupled to the ^{15}N sites through spin–spin interactions. As a result, it is possible to use these spin–spin couplings for hyperpolarization transfer from ^{15}N to ^1H ^[17,60,61] by using conventional polarization trans-

fer techniques such as insensitive nuclei enhanced by polarization transfer (INEPT).^[62] This hyperpolarization transfer approach leads to a large increase in sensitivity of approximately 100-fold, as described above and elsewhere,^[55,57,63] and the speed of imaging readout in the case of MRI and MRSI applications is also enhanced, as described above.

In this work [$^{15}\text{N}_3$]metronidazole was hyperpolarized in alcoholic solution. Although SABRE hyperpolarization in aqueous media has been demonstrated,^[51,64–67] so far, the SABRE polarization levels in aqueous solutions are more than 10-fold lower than those in alcoholic solutions,^[68] for example, in methanol here, largely due to significantly lower H_2 solubility in water.^[69,70] Two potential work-arounds that can be envisioned in the context of biomedical applications are 1) the use of high-pressure hyperpolarizers^[71] to increase the concentration of pH_2 in aqueous solutions or 2) the dilution of alcoholic solutions (e.g., based on ethanol) with a biocompatible buffer followed by in vivo injection, because the ^{15}N T_1 value is nearly 10 minutes in vitro and therefore the slow injection of larger volumes over several minutes may be feasible in the context of future in-human applications.

Conclusion

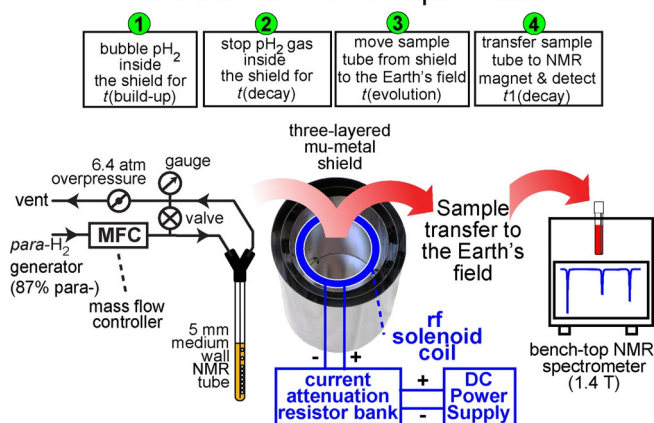
We have demonstrated in this report the ^{15}N SABRE-SHEATH hyperpolarization of [$^{15}\text{N}_3$]metronidazole. Efficient hyperpolarization ($P_{\text{15N}} \approx 16\%$) of the $^{15}\text{NO}_2$ group is accomplished by spin relays created by the network of ^{15}N spins in the molecular structure of [$^{15}\text{N}_3$]metronidazole. In this process, the parahydrogen-derived hyperpolarization of iridium hydrides is transferred over up to six chemical bonds. The high level of nuclear spin polarization P_{15N} of around 16% is achieved in about 1 minute on all three ^{15}N sites of [$^{15}\text{N}_3$]metronidazole at concentrations up to approximately 41 mM. The HP state of the $^{15}\text{NO}_2$ group has a long lifetime in vitro with an exponential decay constant T_1 of 9.7 ± 1.0 minutes at the clinically relevant magnetic field of 1.4 T. Such a long lifetime of the HP state is possible as a result of the low gyromagnetic ratio of the ^{15}N nucleus, and in part because the ^{15}N spin of the $^{15}\text{NO}_2$ group in metronidazole has no detectable spin–spin couplings with any of the protons in the molecule. We have also reported herein on the novel robust synthesis of [$^{15}\text{N}_2$]metronidazole (see the Experimental Section) and [$^{15}\text{N}_3$]metronidazole compounds in a yield of 15% over three steps. This synthetic approach employs inexpensive sources of ^{15}N label ($^{15}\text{NH}_4\text{Cl}$ and $\text{Na}^{15}\text{NO}_3$) and can be potentially tailored for the ^{15}N enrichment of other nitroimidazole derivatives, for example, FDA-approved nimorazole.

Experimental Section

General: The details of the experimental setup (Scheme 2) employed for the studies reported herein have been described previously.^[42,68] All synthetic and spectral characterization details relating to the preparation of [$^{15}\text{N}_2$]metronidazole and [$^{15}\text{N}_3$]metronidazole are provided in the Supporting Information.

SABRE-SHEATH hyperpolarization: The solutions for SABRE hyperpolarization were prepared with a 1:20 catalyst/substrate ratio. A

SABRE-SHEATH Experiment



Scheme 2. Schematic of the experimental setup employed for the SABRE-SHEATH experiments.

known mass of [$^{15}\text{N}_3$]metronidazole was placed in a plastic Eppendorf tube and a 1 mL solution of the Ir-IMes catalyst in [D_4]MeOH (0.6 mL) was added to yield a 20 mM concentration of [$^{15}\text{N}_3$]metronidazole. The mixture was flushed with ultrapure argon gas immediately after preparation. Each solution prepared in this manner was used for SABRE activation and SABRE-SHEATH hyperpolarization experiments typically within 2 h of its initial formulation.

The Ir-IMes catalyst precursor^[39] was synthesized according to our previously published protocol.^[72] The catalyst was activated by pH_2 bubbling for approximately 1 h to achieve maximum performance.

Each sample was placed in a medium-walled 5 mm NMR tube (0.6 mL aliquot) and connected to the SABRE hyperpolarization setup, which has been described in detail previously.^[34,35,42] NMR spectra were recorded by using a 1.4 T benchtop NMR spectrometer (NMR Pro 60, Nanalysis, Canada) with a flow rate of 50 sccm (standard cubic centimeters per minute, the flow rate was controlled by a mass flow controller) and a 6.4 atm overpressure of pH_2 gas in the NMR tube at room temperature (ca. 20–22 °C; Scheme 2). The thermally polarized reference spectrum of neat [^{15}N]pyridine was recorded by ^{15}N NMR spectroscopy with proton decoupling, whereas all ^{15}N NMR spectra of HP [$^{15}\text{N}_3$]metronidazole were recorded under conditions without proton decoupling.

The duration of pH_2 bubbling in the shield was about 1 min (unless otherwise noted), and the durations of $t(\text{decay})$ (< 1 s), $t(\text{evolution})$ (ca. 1–2 s), and sample depolarization in the 1.4 T NMR spectrometer, $t_1(\text{decay})$ (ca. 1–2 s) were kept to a minimum to reduce ^{15}N polarization losses (Figure 1c). Varying the durations of pH_2 bubbling [$t(\text{buildup})$], the polarization decay in the shield after cessation of pH_2 bubbling [$t(\text{decay})$], the evolution of polarization in the Earth's magnetic field [$t(\text{evolution})$], and sample depolarization in the 1.4 T NMR spectrometer [$t_1(\text{decay})$] shown in Scheme 2 allowed for systematic mapping of the SABRE-SHEATH process and the spin dynamics of ^{15}N polarization shown in Figure 2b,e,c,f, respectively. Systematic mapping of the static magnetic field inside the shield (using a variable resistor bank and dc power supply (GW INSTEK, GPRS series), Scheme 2) is shown in Figure 2a.

Some samples were heated to approximately 55 °C to evaporate [D_4]MeOH to increase the concentration of [$^{15}\text{N}_3$]metronidazole for the experiments summarized in Figure 2d.

Preparation of parahydrogen: Parahydrogen (pH_2) enrichment was performed by using a home-made parahydrogen generator

equipped with a SunPower cryocooler. The pH_2 fraction was determined by ^1H NMR spectroscopy as discussed previously.^[10] Briefly, the signal of orthohydrogen in “normal” hydrogen gas (consisting of 75% *ortho* and 25% *para* states) was employed as a signal reference. The orthohydrogen fraction/percentage signal from the pH_2 -enriched mixture was determined next (by using a signal reference obtained from “normal” hydrogen gas) and the fraction/percentage of pH_2 was determined as the difference between 100% and the percentage of detected orthohydrogen. The NMR spectra of normal (25% pH_2) and pH_2 -enriched mixtures are shown in Figure S1 in the Supporting Information. The NMR spectra of several samples were recorded (for reproducibility) and a variability of less than 2% was achieved.

Acknowledgements

This work was supported by the NSF under grants CHE-1836308 (E.Y.C.) and CHE-1416432 (B.M.G.), NIH R21CA220137 (E.Y.C., B.M.G.), DOD CDMRP BRP W81XWH-12-1-0159/BC112431 (E.Y.C., B.M.G., W.P.), DOD PRMRP awards W81XWH-15-1-0271 (E.Y.C.) and W81XWH-15-1-0272 (B.M.G.), and R01CA16700 (W.P.). N.V.C. and K.V.K. thank the Russian Science Foundation (Grant #17-73-20030) for their support in the synthesis of ^{15}N -labeled compounds. I.V.K. thanks the Russian Ministry of Science and Higher Education (Project AAAA-A16-116121510087-5).

Conflict of interest

The authors declare no conflict of interest.

Keywords: hyperpolarization • isotopic labeling • nitrogen heterocycles • NMR spectroscopy • SABRE • spin relays

- [1] P. Nikolaou, B. M. Goodson, E. Y. Chekmenev, *Chem. Eur. J.* **2015**, *21*, 3156–3166.
- [2] P. J. Rayner, M. J. Burns, A. M. Olaru, P. Norcott, M. Fekete, G. G. R. Green, L. A. R. Highton, R. E. Mewis, S. B. Duckett, *Proc. Natl. Acad. Sci. USA* **2017**, *114*, E3188–E3194.
- [3] B. M. Goodson, N. Whiting, A. M. Coffey, P. Nikolaou, F. Shi, B. M. Gust, M. E. Gemeinhardt, R. V. Shchepin, J. G. Skinner, J. R. Birchall, M. J. Barlow, E. Y. Chekmenev, *Emagres* **2015**, *4*, 797–810.
- [4] M. J. Albers, R. Bok, A. P. Chen, C. H. Cunningham, M. L. Zierhut, V. Y. Zhang, S. J. Kohler, J. Tropp, R. E. Hurd, Y.-F. Yen, S. J. Nelson, D. B. Vigneron, J. Kurhanewicz, *Cancer Res.* **2008**, *68*, 8607–8615.
- [5] J. Kurhanewicz, D. B. Vigneron, K. Brindle, E. Y. Chekmenev, A. Comment, C. H. Cunningham, R. J. DeBerardinis, G. G. Green, M. O. Leach, S. S. Rajan, R. R. Rizi, B. D. Ross, W. S. Warren, C. R. Malloy, *Neoplasia* **2011**, *13*, 81–97.
- [6] S. J. Nelson, J. Kurhanewicz, D. B. Vigneron, P. E. Z. Larson, A. L. Harzstark, M. Ferrone, M. van Criekinge, J. W. Chang, R. Bok, I. Park, G. Reed, L. Carvajal, E. J. Small, P. Munster, V. K. Weinberg, J. H. Ardenkjaer-Larsen, A. P. Chen, R. E. Hurd, L. I. Oddegardstuen, F. J. Robb, J. Tropp, J. A. Murray, *Sci. Transl. Med.* **2013**, *5*, 198ra108.
- [7] K. Golman, R. in't Zandt, M. Thaning, *Proc. Natl. Acad. Sci. USA* **2006**, *103*, 11270–11275.
- [8] S. E. Day, M. I. Kettunen, F. A. Gallagher, D. E. Hu, M. Lerche, J. Wolber, K. Golman, J. H. Ardenkjaer-Larsen, K. M. Brindle, *Nat. Med.* **2007**, *13*, 1382–1387.
- [9] M. Merritt, C. Harrison, C. Storey, F. Jeffrey, A. Sherry, C. Malloy, *Proc. Natl. Acad. Sci. USA* **2007**, *104*, 19773–19777.

- [10] J.-B. Hövener, A. N. Pravdivtsev, B. Kidd, C. R. Bowers, S. Glöggler, K. V. Kovtunov, M. Plaumann, R. Katz-Brull, K. Buckenmaier, A. Jerschow, F. Reineri, T. Theis, R. V. Shchepin, S. Wagner, P. Bhattacharya, N. M. Zacharias, E. Y. Chekmenev, *Angew. Chem. Int. Ed.* **2018**, *57*, 11140–11162; *Angew. Chem.* **2018**, *130*, 11310–11333.
- [11] K. M. Brindle, *J. Am. Chem. Soc.* **2015**, *137*, 6418–6427.
- [12] J. H. Ardenkjaer-Larsen, B. Fridlund, A. Gram, G. Hansson, L. Hansson, M. H. Lerche, R. Servin, M. Thaning, K. Golman, *Proc. Natl. Acad. Sci. USA* **2003**, *100*, 10158–10163.
- [13] K. R. Keshari, D. M. Wilson, *Chem. Soc. Rev.* **2014**, *43*, 1627–1659.
- [14] A. Comment, M. E. Merritt, *Biochemistry* **2014**, *53*, 7333–7357.
- [15] J. H. Ardenkjaer-Larsen, *J. Magn. Reson.* **2016**, *264*, 3–12.
- [16] J.-H. Ardenkjaer-Larsen, G. S. Boebinger, A. Comment, S. Duckett, A. S. Edison, F. Engelke, C. Griesinger, R. G. Griffin, C. Hilty, H. Maeda, G. Parigi, T. Prisner, E. Ravera, J. van Buntum, S. Vega, A. Webb, C. Luchinat, H. Schwalbe, L. Frydman, *Angew. Chem. Int. Ed.* **2015**, *54*, 9162–9185; *Angew. Chem.* **2015**, *127*, 9292–9317.
- [17] R. Sarkar, A. Comment, P. R. Vasos, S. Jannin, R. Gruetter, G. Bodenhausen, H. Hall, D. Kirik, V. P. Denisov, *J. Am. Chem. Soc.* **2009**, *131*, 16014–16015.
- [18] W. Jiang, L. Lumata, W. Chen, S. Zhang, Z. Kovacs, A. D. Sherry, C. Khemtong, *Sci. Rep.* **2015**, *5*, 9104.
- [19] A. N. Pravdivtsev, A. V. Yurkovskaya, P. A. Petrov, H.-M. Vieth, K. L. Ivanov, *Appl. Magn. Reson.* **2016**, *47*, 711–725.
- [20] H. Nonaka, R. Hata, T. Doura, T. Nishihara, K. Kumagai, M. Akakabe, M. Tsuda, K. Ichikawa, S. Sando, *Nat. Commun.* **2013**, *4*, 2411.
- [21] J. McCormick, S. Korchak, S. Mamone, Y. N. Ertas, Z. Liu, L. Verlinsky, S. Wagner, S. Glöggler, L.-S. Bouchard, *Angew. Chem. Int. Ed.* **2018**, *57*, 10692–10696; *Angew. Chem.* **2018**, *130*, 10852–10856.
- [22] C. Cudalbu, A. Comment, F. Kurdzesau, R. B. van Heeswijk, K. Uffmann, S. Jannin, V. Denisov, D. Kirik, R. Gruetter, *Phys. Chem. Chem. Phys.* **2010**, *12*, 5818–5823.
- [23] M. Bonnet, C. R. Hong, W. W. Wong, L. P. Liew, A. Shome, J. Wang, Y. Gu, R. J. Stevenson, W. Qi, R. F. Anderson, F. B. Pruijn, W. R. Wilson, S. M. F. Jamieson, K. O. Hicks, M. P. Hay, *J. Med. Chem.* **2018**, *61*, 1241–1254.
- [24] S. Kizaka-Kondoh, H. Konse-Nagasawa, *Cancer Sci.* **2009**, *100*, 1366–1373.
- [25] K. Nepali, H.-Y. Lee, J.-P. Liou, *J. Med. Chem.* **2019**, *62*, 2851–2893.
- [26] R. W. Adams, J. A. Aguilar, K. D. Atkinson, M. J. Cowley, P. I. P. Elliott, S. B. Duckett, G. G. R. Green, I. G. Khazal, J. Lopez-Serrano, D. C. Williamson, *Science* **2009**, *323*, 1708–1711.
- [27] R. W. Adams, S. B. Duckett, R. A. Green, D. C. Williamson, G. G. R. Green, *J. Chem. Phys.* **2009**, *131*, 194505.
- [28] K. D. Atkinson, M. J. Cowley, S. B. Duckett, P. I. P. Elliott, G. G. R. Green, J. López-Serrano, I. G. Khazal, A. C. Whitwood, *Inorg. Chem.* **2009**, *48*, 663–670.
- [29] K. D. Atkinson, M. J. Cowley, P. I. P. Elliott, S. B. Duckett, G. G. R. Green, J. Lopez-Serrano, A. C. Whitwood, *J. Am. Chem. Soc.* **2009**, *131*, 13362–13368.
- [30] P. J. Rayner, S. B. Duckett, *Angew. Chem. Int. Ed.* **2018**, *57*, 6742–6753; *Angew. Chem.* **2018**, *130*, 6854–6866.
- [31] S. Knecht, A. N. Pravdivtsev, J.-B. Hövener, A. V. Yurkovskaya, K. L. Ivanov, *RSC Adv.* **2016**, *6*, 24470–24477.
- [32] A. N. Pravdivtsev, A. V. Yurkovskaya, H. Zimmermann, H.-M. Vieth, K. L. Ivanov, *RSC Adv.* **2015**, *5*, 63615–63623.
- [33] B. J. A. van Weerdenburg, S. Glöggler, N. Eshuis, A. H. J. Engwerda, J. M. M. Smits, R. de Gelder, S. Appelt, S. S. Wymenga, M. Tessari, M. C. Feiters, B. Blumich, F. P. J. T. Rutjes, *Chem. Commun.* **2013**, *49*, 7388–7390.
- [34] T. Theis, M. L. Truong, A. M. Coffey, R. V. Shchepin, K. W. Waddell, F. Shi, B. M. Goodson, W. S. Warren, E. Y. Chekmenev, *J. Am. Chem. Soc.* **2015**, *137*, 1404–1407.
- [35] M. L. Truong, T. Theis, A. M. Coffey, R. V. Shchepin, K. W. Waddell, F. Shi, B. M. Goodson, W. S. Warren, E. Y. Chekmenev, *J. Phys. Chem. C* **2015**, *119*, 8786–8797.
- [36] B. E. Kidd, J. L. Gesiorski, M. E. Gemeinhardt, R. V. Shchepin, K. V. Kovtunov, I. V. Koptyug, E. Y. Chekmenev, B. M. Goodson, *J. Phys. Chem. C* **2018**, *122*, 16848–16852.
- [37] D. A. Barskiy, R. V. Shchepin, A. M. Coffey, T. Theis, W. S. Warren, B. M. Goodson, E. Y. Chekmenev, *J. Am. Chem. Soc.* **2016**, *138*, 8080–8083.
- [38] J. F. P. Colell, A. W. J. Logan, Z. Zhou, R. V. Shchepin, D. A. Barskiy, G. X. Ortiz, Q. Wang, S. J. Malcolmson, E. Y. Chekmenev, W. S. Warren, T. Theis, *J. Phys. Chem. C* **2017**, *121*, 6626–6634.
- [39] M. J. Cowley, R. W. Adams, K. D. Atkinson, M. C. R. Cockett, S. B. Duckett, G. G. R. Green, J. A. B. Lohman, R. Kerssebaum, D. Kilgour, R. E. Mewis, *J. Am. Chem. Soc.* **2011**, *133*, 6134–6137.
- [40] D. A. Barskiy, R. V. Shchepin, C. P. N. Tanner, J. F. P. Colell, B. M. Goodson, T. Theis, W. S. Warren, E. Y. Chekmenev, *ChemPhysChem* **2017**, *18*, 1493–1498.
- [41] R. V. Shchepin, L. Jaigirdar, T. Theis, W. S. Warren, B. M. Goodson, E. Y. Chekmenev, *J. Phys. Chem. C* **2017**, *121*, 28425–28434.
- [42] R. V. Shchepin, L. Jaigirdar, E. Y. Chekmenev, *J. Phys. Chem. C* **2018**, *122*, 4984–4996.
- [43] B. Kidd, J. Mashni, M. Limbach, F. Shi, E. Y. Chekmenev, Y. Hou, B. M. Goodson, *Chem. Eur. J.* **2018**, *24*, 10641–10645.
- [44] A. S. Kiryutin, A. V. Yurkovskaya, H. Zimmermann, H.-M. Vieth, K. L. Ivanov, *Magn. Reson. Chem.* **2018**, *56*, 651–662.
- [45] R. V. Shchepin, M. L. Truong, T. Theis, A. M. Coffey, F. Shi, K. W. Waddell, W. S. Warren, B. M. Goodson, E. Y. Chekmenev, *J. Phys. Chem. Lett.* **2015**, *6*, 1961–1967.
- [46] M. H. Levitt, *J. Magn. Reson.* **2016**, *262*, 91–99.
- [47] J. Kurhanewicz, D. B. Vigneron, J. H. Ardenkjaer-Larsen, J. A. Bankson, K. Brindle, C. H. Cunningham, F. A. Gallagher, K. R. Keshari, A. Kjaer, C. Laustsen, D. A. Mankoff, M. E. Merritt, S. J. Nelson, J. M. Pauly, P. Lee, S. Ronen, D. J. Tyler, S. S. Rajan, D. M. Spielman, L. Wald, X. Zhang, C. R. Malloy, R. Rizi, *Neoplasia* **2019**, *21*, 1–16.
- [48] R. V. Shchepin, D. A. Barskiy, A. M. Coffey, M. A. Feldman, L. M. Kovtunova, V. I. Bukhtiyarov, K. V. Kovtunov, B. M. Goodson, I. V. Koptyug, E. Y. Chekmenev, *ChemistrySelect* **2017**, *2*, 4478–4483.
- [49] S. H. Erickson, G. L. Oppenheim, G. H. Smith, *Obstet. Gynecol.* **1981**, *57*, 48–50.
- [50] K. V. Kovtunov, L. M. Kovtunova, M. E. Gemeinhardt, A. V. Bukhtiyarov, J. Gesiorski, V. I. Bukhtiyarov, E. Y. Chekmenev, I. V. Koptyug, B. M. Goodson, *Angew. Chem. Int. Ed.* **2017**, *56*, 10433–10437; *Angew. Chem.* **2017**, *129*, 10569–10573.
- [51] J. F. P. Colell, M. Emondts, A. W. J. Logan, K. Shen, J. Bae, R. V. Shchepin, G. X. Ortiz, P. Spanring, Q. Wang, S. J. Malcolmson, E. Y. Chekmenev, M. C. Feiters, F. P. J. T. Rutjes, B. Blumich, T. Theis, W. S. Warren, *J. Am. Chem. Soc.* **2017**, *139*, 7761–7767.
- [52] K. Hendrickson, M. Phillips, W. Smith, L. Peterson, K. Krohn, J. Rajendran, *Radiother. Oncol.* **2011**, *101*, 369–375.
- [53] Y. Masaki, Y. Shimizu, T. Yoshioka, Y. Tanaka, K.-i. Nishijima, S. Zhao, K. Higashino, S. Sakamoto, Y. Numata, Y. Yamaguchi, N. Tamaki, Y. Kuge, *Sci. Rep.* **2015**, *5*, 16802.
- [54] J. L. Bolton, R. A. McClelland, *J. Am. Chem. Soc.* **1989**, *111*, 8172–8181.
- [55] D. I. Hoult, R. E. Richards, *J. Magn. Reson. (1969)* **1976**, *24*, 71–85.
- [56] A. M. Coffey, K. V. Kovtunov, D. Barskiy, I. V. Koptyug, R. V. Shchepin, K. W. Waddell, P. He, K. A. Groome, Q. A. Best, F. Shi, B. M. Goodson, E. Y. Chekmenev, *Anal. Chem.* **2014**, *86*, 9042–9049.
- [57] J. Wang, F. Kreis, A. J. Wright, R. L. Hesketh, M. H. Levitt, K. M. Brindle, *Magn. Reson. Med.* **2018**, *79*, 741–747.
- [58] M. L. Truong, A. M. Coffey, R. V. Shchepin, K. W. Waddell, E. Y. Chekmenev, *Contrast Media Mol. Imaging* **2014**, *9*, 333–341.
- [59] M. Mishkovsky, T. Cheng, A. Comment, R. Gruetter, *Magn. Reson. Med.* **2012**, *68*, 349–352.
- [60] J. A. Pfeilsticker, J. E. Ollerenshaw, V. A. Norton, D. P. Weitekamp, *J. Magn. Reson.* **2010**, *205*, 125–129.
- [61] V. A. Norton, D. P. Weitekamp, *J. Chem. Phys.* **2011**, *135*, 141107.
- [62] G. A. Morris, R. Freeman, *J. Am. Chem. Soc.* **1979**, *101*, 760–762.
- [63] D. I. Hoult, P. C. Lauterbur, *J. Magn. Reson. (1969)* **1979**, *34*, 425–433.
- [64] H. Zeng, J. Xu, M. T. McMahon, J. A. B. Lohman, P. C. M. van Zijl, *J. Magn. Reson.* **2014**, *246*, 119–121.
- [65] J.-B. Hövener, N. Schwaderlapp, R. Borowiak, T. Lickert, S. B. Duckett, R. E. Mewis, R. W. Adams, M. J. Burns, L. A. R. Highton, G. G. R. Green, A. Orlaru, J. Hennig, D. von Elverfeldt, *Anal. Chem.* **2014**, *86*, 1767–1774.
- [66] R. V. Shchepin, D. A. Barskiy, A. M. Coffey, T. Theis, F. Shi, W. S. Warren, B. M. Goodson, E. Y. Chekmenev, *ACS Sens.* **2016**, *1*, 640–644.
- [67] P. Spanring, I. Reile, M. Emondts, P. P. M. Schleker, N. K. J. Hermkens, N. G. J. van der Zwaluw, B. J. A. van Weerdenburg, P. Tinnemans, M. Tessari, B. Blümich, F. P. J. T. Rutjes, M. C. Feiters, *Chem. Eur. J.* **2016**, *22*, 9277–9282.

- [68] M. L. Truong, F. Shi, P. He, B. Yuan, K. N. Plunkett, A. M. Coffey, R. V. Shchepin, D. A. Barskiy, K. V. Kovtunov, I. V. Koptug, K. W. Waddell, B. M. Goodson, E. Y. Chekmenev, *J. Phys. Chem. B* **2014**, *118*, 13882–13889.
- [69] M. Herskowitz, J. Wisniak, L. Skladman, *J. Chem. Eng. Data* **1983**, *28*, 164–166.
- [70] Purwanto, R. M. Deshpande, R. V. Chaudhari, H. Delmas, *J. Chem. Eng. Data* **1996**, *41*, 1414–1417.
- [71] A. M. Coffey, R. V. Shchepin, B. Feng, R. D. Colon, K. Wilkens, K. W. Waddell, E. Y. Chekmenev, *J. Magn. Reson.* **2017**, *284*, 115–124.
- [72] D. A. Barskiy, K. V. Kovtunov, I. V. Koptug, P. He, K. A. Groome, Q. A. Best, F. Shi, B. M. Goodson, R. V. Shchepin, A. M. Coffey, K. W. Waddell, E. Y. Chekmenev, *J. Am. Chem. Soc.* **2014**, *136*, 3322–3325.

Manuscript received: March 13, 2019
Revised manuscript received: April 4, 2019
Accepted manuscript online: April 9, 2019
Version of record online: May 30, 2019